Cell volume change through water efflux impacts cell stiffness and stem cell fate

Ming Guo[a,1], Adrian F. Pegoraro[a], Angelo Mao[a,b], Enhua H. Zhou[c,2], Praveen R. Arany[d,e], Yulong Han[a,f], Dylan T. Burnette[g], Mikkel H. Jensen[a,h], Karen E. Kasza[a,i], Jeffrey R. Moore[j], Frederick C. Mackintosh[k,l,m], Jeffrey J. Fredberg[c], David J. Mooney[a,b], Jennifer Lippincott-Schwartz[n,3], and David A. Weitz[a,o,3]

[a]John A. Paulson School of Engineering and Applied Sciences, Harvard University, Cambridge, MA 02138; [b]Wyss Institute for Biologically Inspired Engineering, Harvard University, Cambridge, MA 02138; [c]Harvard T. H. Chan School of Public Health, Boston, MA 02115; [d]Department of Oral Biology, University at Buffalo, Buffalo, NY 14214; [e]Department of Biomedical Engineering, University at Buffalo, Buffalo, NY 14214; [f]Biomedical Engineering and Biomechanics Center, Xi'an Jiaotong University, Xi'an 710049, China; [g]Department of Cell and Developmental Biology, Vanderbilt University School of Medicine, Nashville, TN 37232; [h]Department of Physics and Astronomy, California State University, Sacramento, CA 95819; [i]Department of Mechanical Engineering, Columbia University, New York, NY 10027; [j]Department of Biological Sciences, University of Massachusetts at Lowell, Lowell, MA 01854; [k]Department of Physics and Astronomy, VU University, 1081 HV Amsterdam, The Netherlands; [l]Department of Chemical and Biomolecular Engineering, Rice University, Houston, TX 77030; [m]Center for Theoretical Biophysics, Rice University, Houston, TX 77030; [n]Howard Hughes Medical Institute, Janelia Research Campus, Ashburn, VA 20147; and [o]Department of Physics, Harvard University, Cambridge, MA 02138

Contributed by Jennifer Lippincott-Schwartz, August 26, 2017 (sent for review March 29, 2017; reviewed by Daniel A. Fletcher and Valerie M. Weaver)

Cells alter their mechanical properties in response to their local microenvironment; this plays a role in determining cell function and can even influence stem cell fate. Here, we identify a robust and unified relationship between cell stiffness and cell volume. As a cell spreads on a substrate, its volume decreases, while its stiffness concomitantly increases. We find that both cortical and cytoplasmic cell stiffness scale with volume for numerous perturbations, including varying substrate stiffness, cell spread area, and external osmotic pressure. The reduction of cell volume is a result of water efflux, which leads to a corresponding increase in intracellular molecular crowding. Furthermore, we find that changes in cell volume, and hence stiffness, alter stem-cell differentiation, regardless of the method by which these are induced. These observations reveal a surprising, previously unidentified relationship between cell stiffness and cell volume that strongly influences cell biology.

cell volume | cell mechanics | molecular crowding | gene expression | stem cell fate

Cell volume is a highly regulated property that affects myriad functions (1, 2). It changes over the course of the cell life cycle, increasing as the cell plasma membrane grows and the amount of protein, DNA, and other intracellular material increases (3). However, it can also change on a much more rapid time scale, as, for example, on cell migration through confined spaces (4, 5); in this case, the volume change is a result of water transport out of the cell. This causes increased concentration of intracellular material and molecular crowding, having numerous important consequences (6, 7). Alternately, the volume of a cell can be directly changed through application of an external osmotic pressure. This forces water out of the cell, which also decreases cell volume, increases the concentration of intracellular material, and intensifies molecular crowding. Application of an external osmotic pressure to reduce cell volume also has other pronounced manifestations: For example, it leads to a significant change in cell mechanics, resulting in an increase in stiffness (8); it also impacts folding and transport of proteins (9), as well as condensation of chromatin (10). These dramatic effects of osmotic-induced volume change on cell behavior raise the question of whether cells ever change their volume through water efflux under isotonic conditions, perhaps to modulate their mechanics and behavior through changes in molecular crowding.

Here, we demonstrate that when cells are cultured under the same isotonic conditions, but under stiffer extracellular environments, they reduce their cell volume through water efflux out of the cell, and this has a large and significant impact on cell mechanics and cell physiology. Specifically, as a cell spreads out on a stiff substrate, its volume decreases, and the cell behaves in a similar manner to that observed for cells under external osmotic pressure: Both the cortical and cytoplasmic stiffness increase as the volume decreases; the nuclear volume also decreases as cell volume decreases. Moreover, stem-cell differentiation is also strongly impacted by cell volume changes. These results suggest that cells in different environments can change their volume through water efflux. This leads to changes in molecular crowding and impacts the mechanics, physiology, and behavior of the cell, having far-reaching consequences on cell fate.

Results

Bulk and Shear Moduli of Cells Increase as Cell Volume Decreases Under External Osmotic Compression. To directly probe the consequences of changes in cell volume, we control the external osmotic pressure through the addition of 300-Da polyethylene glycol (PEG 300) (8, 11). We measure the cell volume by fluorescently labeling

Significance

Cell volume is thought to be a well-controlled cellular characteristic, increasing as a cell grows, while macromolecular density is maintained. We report that cell volume can also change in response to external physical cues, leading to water influx/efflux, which causes significant changes in subcellular macromolecular density. This is observed when cells spread out on a substrate: Cells reduce their volume and increase their molecular crowding due to an accompanying water efflux. Exploring this phenomenon further, we removed water from mesenchymal stem cells through osmotic pressure and found this was sufficient to alter their differentiation pathway. Based on these results, we suggest cells chart different differentiation and behavioral pathways by sensing/altering their cytoplasmic volume and density through changes in water influx/efflux.

Author contributions: M.G., J.L.-S., and D.A.W. designed research; M.G., A.F.P., A.M., E.H.Z., P.R.A., Y.H., D.T.B., and K.E.K. performed research; M.G., A.M., E.H.Z., P.R.A., D.T.B., M.H.J., K.E.K., J.R.M., and D.J.M. contributed new reagents/analytic tools; M.G., A.F.P., Y.H., F.C.M., J.J.F., and D.A.W. analyzed data; and M.G., A.F.P., J.L.-S., and D.A.W. wrote the paper.

Reviewers: D.A.F., University of California, Berkeley; and V.M.W., University of California, San Francisco.

The authors declare no conflict of interest.

[1]Present address: Department of Mechanical Engineering, Massachusetts Institute of Technology, Cambridge, MA 02139.

[2]Present address: Ophthalmology, Novartis Institutes of BioMedical Research, Cambridge, MA 02139.

[3]To whom correspondence may be addressed. Email: lippincottschwartzj@janelia.hhmi.org or weitz@seas.harvard.edu.

This article contains supporting information online at www.pnas.org/lookup/suppl/doi:10.1073/pnas.1705179114/-/DCSupplemental.

the cytoplasm and cell surface and use confocal microscopy to identify the boundaries of the cell in 3D (12, 13). The measured volumes have been shown to be consistent with those measured by atomic force microscopy (AFM) (8). We further validate our confocal measurements by comparing them to those made by using high-resolution structured illumination microscopy (SIM) on the same sample; the measured cell volumes are consistent for both techniques, indicating a measurement uncertainty of <10% (Fig. S1). Because cell volume naturally changes during the cell cycle, we make all our observations after starving cells overnight; however, measurements made under standard culture conditions exhibit the same behavior, albeit with increased variability.

To explore the dependence of cell volume on external osmotic pressure, we culture A7 cells on glass substrates and add increasing concentrations of PEG 300 to the medium; PEG 300 does not penetrate the cell membrane and thus increases the external osmotic pressure. Since the osmotic pressure imbalance across the cell cortex is negligible (14), the external osmotic pressure must be matched by the internal osmotic pressure, which is controlled by the concentration of ions and small proteins. Thus, to compensate for the increase of external osmotic pressure, the cell must increase its internal osmolyte concentration either by ion influx or water efflux. We find that the cell volume decreases with increasing external osmotic pressure (Fig. S2). This must be due to water efflux, because the cell volume recovers its original value upon removal of the external osmotic pressure. Cells eventually reach a minimum volume under extreme osmotic compression (Fig. S2); this reflects the volume of the total intracellular material, as well as any osmotically inactive water required to hydrate ions and proteins. This behavior is reminiscent of an ideal gas system with an excluded volume, where the pressure is purely entropic in origin. Indeed, the relationship between osmotic pressure P and cell volume V is consistent with $P = Nk_BT/(V - V_{min})$, where N is the number of intracellular osmolytes, k_B is the Boltzmann constant, T is the absolute temperature, and V_{min} is the minimum volume (8). To confirm that the decrease in cell volume is due to water efflux, we use the Bradford assay to measure the total protein content per cell before and after osmotic compression and find no significant difference (*SI Materials and Methods*).

As cell volume decreases, it becomes increasingly difficult to remove additional water and further shrink the cell because the concentration of intracellular ions and other materials increases. The resistance of water leaving a cell is the osmotic bulk modulus and is defined as $B = -V\mathrm{d}P/\mathrm{d}V \sim -V\Delta P/\Delta V$. By varying the osmotic pressure and measuring the resultant volume of A7 cells cultured on a glass substrate, we measure B and find that it increases as cell volume decreases, as shown by the points at the top in Fig. 1*A*. Using the expression for the volume dependence of P, we can predict the behavior of the bulk modulus, $B = Nk_BTV/(V - V_{min})^2$. This functional form provides an excellent fit to the data, as shown by the dashed line through the points at the top in Fig. 1*A*. The value of V_{min} determined by the fit is 2,053 ± 30 μm^3; this agrees with the minimum volume measured when the cells are exposed to extreme osmotic compression to remove all osmotically active water, ~2,100 μm^3. The fit also provides a value for N, and this gives a concentration of ~200 mM, which is consistent with the known salt concentration within a cell (15). The excellent fitting with a constant N suggests that the total amounts of ions and proteins remain approximately constant during osmotic compression. While the osmotic pressure balance is largely controlled by ion concentration, the concentration of large proteins and organelles also increases as free water leaves the cell. It is the volume of these proteins and organelles (including the nucleus) that predominantly determines V_{min}. Moreover, as the cell approaches its minimum volume, molecular crowding must increase within the cell, and this might lead to additional changes in cell behavior.

Among many cell properties, cortical stiffness has been shown to depend on volume through molecular crowding as cells are osmotically compressed (8). To measure changes in cortical stiffness, we use optical magnetic twisting cytometry (OMTC) to determine the cortical shear modulus, G, of A7 cells, as shown in Fig. S3 (8, 16, 17); the results obtained with OMTC are in quantitative agreement with those obtained by using AFM (18, 19). The cortical shear modulus and the volume both change rapidly, but simultaneously, as the external osmotic pressure is increased, as shown in Fig. 1*B*; moreover, the cortical shear modulus recovers its initial value immediately upon removal of the external osmotic pressure (Fig. S2*B*). Interestingly, the cell cortical stiffness has the same trend as the bulk modulus and is described by exactly the same functional form as shown by the points and dashed line, respectively, in the middle of Fig. 1*A*. The value of V_{min} obtained by fitting the functional form to the data, 2,004 ± 41 μm^3, agrees well with that obtained from the fit to the bulk modulus. However, the value of the shear modulus is consistently three orders of magnitude less than that of the bulk modulus. The similar

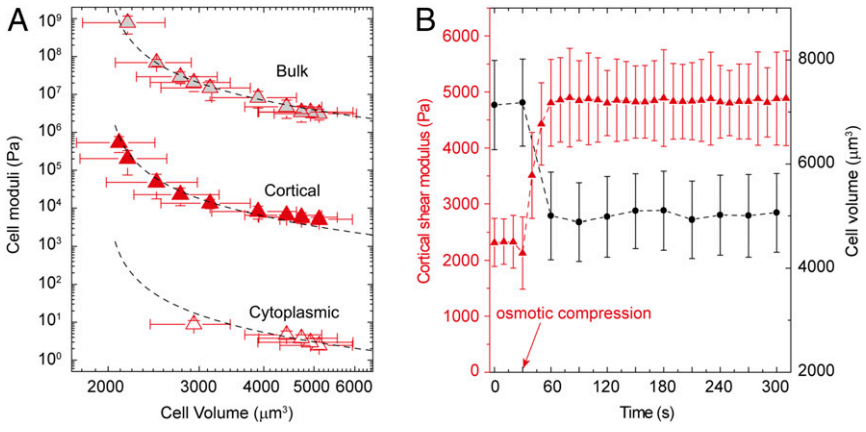

Fig. 1. Mechanical properties of A7 cells on glass as a function of cell volume under external osmotic pressures. (*A*) Osmotic bulk modulus (gray triangles), cortical shear modulus (red triangles), and cytoplasmic shear modulus (open triangles) increase as cell volume is decreased upon external osmotic compression. The dashed line through gray triangles represents the least-squares fit using the functional form, $B = Nk_BTV/(V - V_{min})^2$ ($R^2 = 0.99$). Dashed lines through the cortical and cytoplasmic moduli are exactly the same fit, simply scaled by a factor of 500 and 100,000, respectively. (*B*) Cortical shear modulus of a single A7 cell, measured by OMTC, increases immediately after the application of an osmotic compression with 0.26 M PEG 300; this is concurrent with a decrease in cell volume after osmotic compression.

dependence of the shear and bulk moduli on cell volume implies that molecular crowding has the dominant effect on both.

The major contribution of the shear modulus of the cell comes from the cortical stiffness. However, the cell is a highly heterogeneous structure, and the interior is much softer; the cytoplasm of the cell is a weak elastic gel with a shear modulus that is three orders of magnitude lower than that of the cortex (17, 20). To measure cytoplasmic stiffness, we microinject PEG-coated polystyrene beads into A7 cells and use laser tweezers to determine the cytoplasmic shear modulus, as shown in Fig. S3 (*Materials and Methods*). The intracellular shear modulus increases as cell volume decreases, following an identical trend as both the cortical shear and bulk moduli, as shown by the lower points in Fig. 1*A*. The cytoplasmic shear modulus clearly increases as the cell volume is further decreased, but its value is too large to be measured with the laser tweezers. Over the range accessible, the cytoplasmic shear modulus behavior has the same functional form as do the other two moduli, as shown by the dashed line at the bottom of Fig. 1*A*; however, its value is a further three orders of magnitude less than that of the cortical shear modulus.

Cells Reduce Their Volume When Cultured on Stiffer Substrates. Cortical stiffness is a key physical property of cell mechanics, and its value typically decreases as the stiffness of the substrate on which the cells are grown decreases (21). Cell morphology can vary markedly with substrate stiffness, and this could also impact molecular crowding, even under isotonic conditions. To investigate this possibility, we culture A7 cells on 100-μm-thick polyacrylamide (PA) gels coated with collagen I; by varying gel composition, we tune the shear modulus of the gels from 0.1 to 10 kPa, matching the physiological elasticities of natural tissues (Table S1). To probe cell morphology, we measure the cell spread area; it increases significantly for cells cultured on stiffer substrates (21–24), as shown by the confocal images in Fig. 2*A*, *Upper*, and as summarized in Fig. 2*B*. Surprisingly, however, cell volume is not conserved: As substrate rigidity increases, cell volume decreases. On the most rigid substrates, the volume decrease is as much as ~40% compared with cells grown on the softest substrates where their volume is a maximum, as shown in Fig. 2*C*. Other mammalian cell types, including HeLa, NIH 3T3, mouse mesenchymal stem cell (mMSCs), and primary human airway smooth muscle cells, show similar behavior (Fig. 2*C*). This confirms the generality of the dependence of cell volume on substrate stiffness. Thus, even without changes in external osmotic pressure, the cell volume can change.

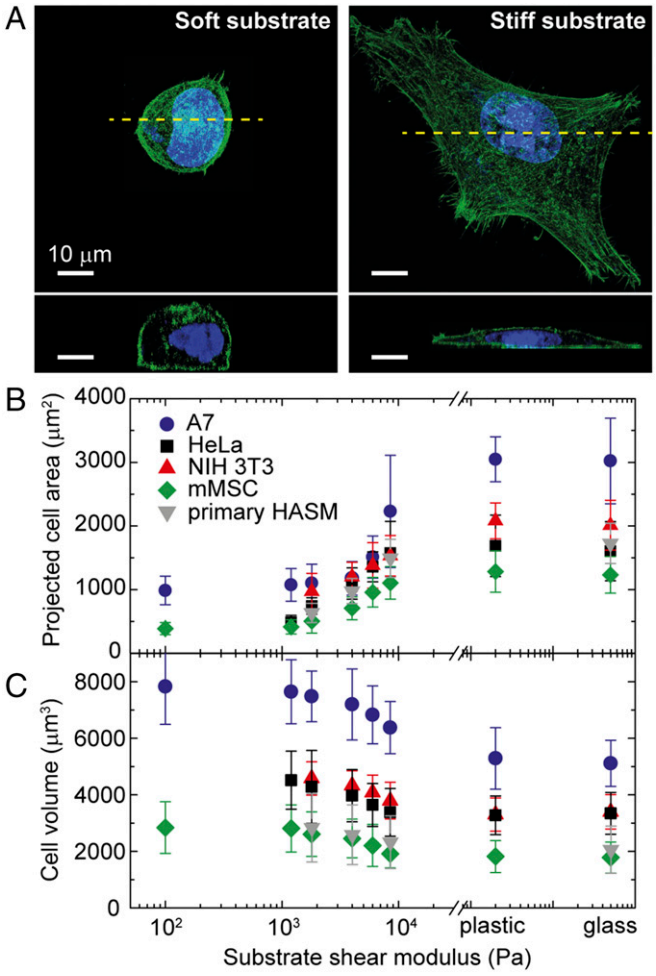

Fig. 2. Morphology and volume of adherent cells change with increasing substrate stiffness. (*A*) Top and side views of fixed A7 cells on a stiff (shear modulus of 10 kPa) and a soft (shear modulus of 1,200 Pa) PA gel substrate coated with collagen I. The actin cortex (green) and nucleus (blue) are labeled. (*B*) The projected cell area increases with increasing substrate stiffness. (*C*) Cell volume markedly decreases with increasing substrate stiffness. Error bars represent the SD ($n > 200$ individual cells). HASM, human airway smooth muscle.

Restricting Spread Area Increases Cell Volume. To further explore the nature of the change in cell volume with substrate stiffness, we investigate the role of spread area. We culture A7 cells on a glass substrate, but control the spread area by restricting their adhesion. We micropattern collagen "islands" of varying size on a glass substrate to limit the adhesion area of the cells (25). Interestingly, we find that cells with limited spread area have a larger height compared with cells with unrestricted spread area (Fig. 3*A*). Moreover, the cell volume also increases as the spread area decreases, as shown in Fig. 3*B*. The same effect is observed when we grow cells on micropatterned softer substrates: If the cell spread area is restricted to be less than that of a freely spreading cell on the substrate, the volume increases. Remarkably, cell volume exhibits the same dependence on spread area regardless of how the area is attained, either through controlling the adhesive area on a stiff substrate or through varying substrate stiffness, as shown by the comparison of the blue and gray points in Fig. 3*C*.

Cell Volume Reduction Is Due to Intracellular Water Efflux. To determine whether the reduction in cell volume under isotonic conditions is due to changes in protein content or to water efflux, we monitor a single trypsinized cell as it spreads on a rigid substrate. The cell changes from its initial rounded state to a fully spread state in ~20 min. During this time period, the cell volume decreases concomitantly with increasing spread area, as shown in Fig. 3*D*. The relationship between volume and spread area is identical to that of cells cultured on confined areas or on substrates of varying rigidities, as shown by the red × symbols in Fig. 3*C*. Water can leave the cell within a minute (8, 26), while changes in amount of intracellular materials due to growth can typically take hours for mammalian cells (3, 27). Thus, these results suggest that volume reduction under isotonic conditions is most likely controlled through water exchange, albeit at isotonic osmotic pressure.

To confirm that cell volume variation upon spreading is due to water efflux and not protein loss, we measure the total protein content per cell for cells cultured on both stiff and soft substrates and find no significant difference (*SI Materials and Methods*). Consistent with this, when we apply extreme osmotic pressure to cells by exchanging culture medium with pure PEG, thereby extracting all osmotically active water from the cells, we find that the resultant minimum volume, V_{min}, is independent of substrate stiffness (Fig. 4). Since V_{min} approximately reflects the amount of intracellular material and bound water that is osmotically inactive

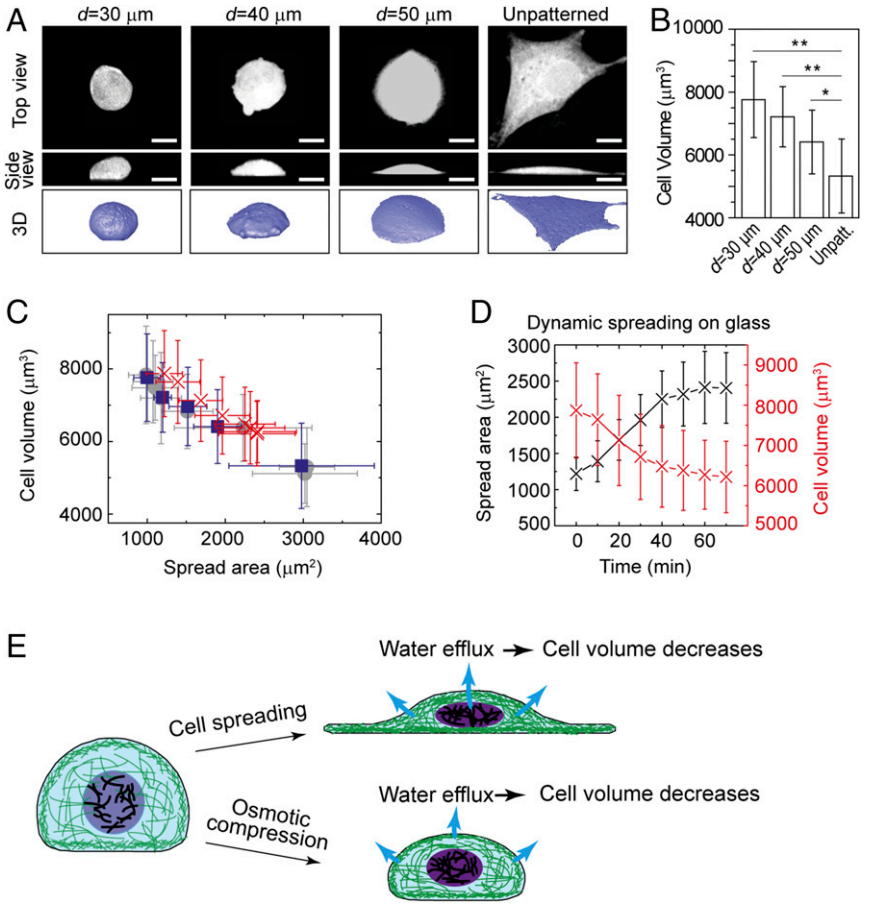

Fig. 3. Cell volume of A7 cells increases when the cell spread area is decreased by growing cells on micropatterned collagen islands. Error bars represent the SD. *$P < 0.05$; **$P < 0.01$. (*A*) Shown are 3D images of A7 cells on micropatterned islands of different sizes on glass. Cells are labeled with cell tracker green. (Scale bars, 20 μm.) (*B*) Cell volume decreases with increasing cell spread area on glass. (*C*) Cell volume plotted as a function of the projected area, for cells on substrates with different stiffnesses (gray circles; $n > 200$), cells on a glass substrate but with different available spread area (blue squares; $n > 200$), and a dynamically spreading cell (red crosses; $n = 3$). (*D*) Variation of cell spread area and volume as a single cell dynamically attaches on a stiff substrate ($n = 3$). (*E*) Schematic illustration of cell volume decrease through water efflux, as cells spread out or are osmotically compressed.

(8), these data support the view that variation of cell volume results from exchange of free intracellular water.

Ion Channels and the Actomyosin Cytoskeleton Play a Role in Cell Volume Reduction During Spreading. The efflux of water during cell spreading under isotonic conditions must have a different origin than the efflux of water during osmotic compression. In both cases, the osmotic pressure is balanced across the cell membrane. Under osmotic compression, the total amount of material, including ions and proteins, remains approximately constant; the internal osmotic pressure increases as a result of increasing intracellular osmolyte concentration through water efflux. During

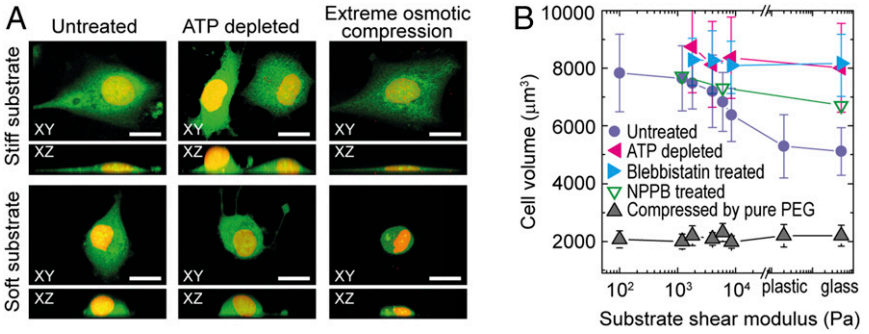

Fig. 4. Cell morphology and volume under drug treatment and osmotic compression. (*A*) The 3D morphology of control cells and cells with ATP depletion and under extreme osmotic compression, on stiff and soft substrates. Cytoplasm (green) and nucleus (yellow) are labeled. (Scale bars: 20 μm.) (*B*) Cells without active contraction (blebbistatin-treated and ATP-depleted) and under extreme osmotic compression do not exhibit a volume dependence with substrate stiffness; cells with choloride channels-inhibited (NPPB treated) exhibit a weaker volume dependence with substrate stiffness. The control data of A7 cells is same as in Fig. 2*C*. Error bars represent the SD ($n > 200$ individual cells).

cell spreading, cell volume reduction occurs under isotonic conditions; for water to leave the cell, the total amount of osmolytes must change. Since the amount of protein per cell remains constant, it is instead likely the reduction of osmolytes for cells on stiff substrates is due to the exchange of ions with the surroundings. During cell spreading, cytoskeletal tension increases, and this has been tied to the increase of ion channel activity (28–30). To test the role of ion channel activity on cell volume variation, we inhibit chloride ion channels by 0.1 mM 5-nitro-2-(3-phenylpropylamino)-benzoic acid (NPPB) after cells fully spread. The decrease in cell volume with increasing substrate stiffness is significantly suppressed when ion channels are blocked, as shown by the green open triangles in Fig. 4*B*. This indicates that cell volume reduction under isotonic conditions requires the activity of ion channels to change the total amount of internal osmolytes and hence ensure that the osmotic pressure remains balanced.

To further test if active cell processes play a role in the reduction of cell volume, we treat cells with 10 μM blebbistatin to inhibit myosin II motor activity and thus directly reduce cytoskeletal tension. Blebbistatin treatment prevents cells from decreasing their volume on stiff substrates, as shown by the blue triangles in Fig. 4*B*. The same increase in volume is observed when we inhibit general motor activity by depleting ATP using 2 mM sodium azide and 10 mM 2-deoxyglucose, as shown by the pink triangles in Fig. 4*B*. These results further demonstrate that active cellular processes are involved in volume decrease under isotonic conditions and that cells must actively control the osmolyte concentration using ion channels to affect water efflux and change their volume.

Cell Moduli Demonstrate a Universal Dependence on Cell Volume. Cell cortical stiffness increases with substrate stiffness as the cells increase their spread area under isotonic conditions; cell cortical stiffness also increases as we change the spread area for fixed substrate stiffness. However, cell stiffness also increases for fixed substrate stiffness and fixed spread area when the osmotic pressure is increased, thereby decreasing cell volume. We therefore hypothesize that cell volume change is the common descriptor underlying the cell stiffness change observed in all these cases. To investigate this hypothesis, we plot cortical stiffness as a function of volume: Cell stiffness decreases with increasing volume as cells are grown on softer substrates (Fig. 5*A*). Cell stiffness decreases in a similar fashion with increasing volume as cells are grown on a substrate with fixed stiffness, but with varying adhesive areas (Fig. 5*B*). Similarly, cell stiffness increases as cells grown on a soft substrate are compressed by an external osmotic pressure (Fig. 5*C*) and when cells grown on a stiff substrate and a highly constrained area are compressed through osmotic pressure (Fig. 5*D*). Remarkably, when we plot all these data on a single graph (Fig. 5*E*), they all overlay and exhibit a universal dependency between cell stiffness and cell volume across all perturbations. Thus, cell volume change is indeed a common descriptor of cell stiffness

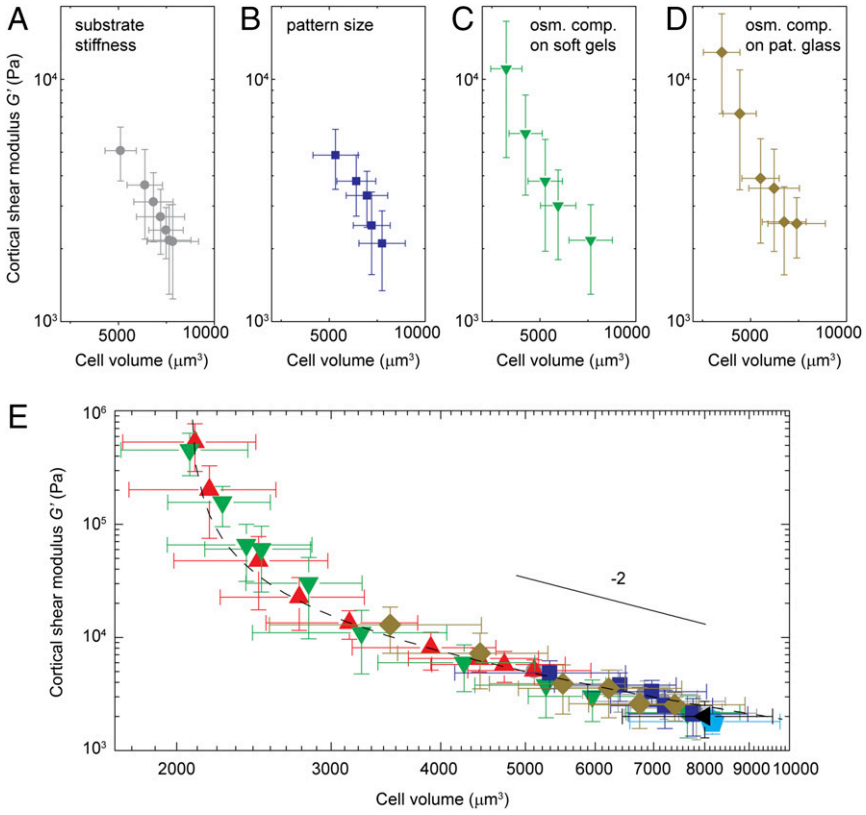

Fig. 5. Relationship of cell cortical stiffness and cell volume. (*A–D*) Dependence of cell cortex shear modulus of A7 cells on their volume, under different conditions, including cells cultured on substrates of varying stiffnesses (*A*), on a stiff substrate with micropatterns of varying sizes (*B*), on a soft substrate with a shear modulus of 100 Pa with addition of increasing amount of osmotic pressure (*C*), and on a glass substrate with small micropatterns limiting cell spreading and with the addition of osmotic pressures (*D*). (*E*) Cell cortical shear modulus scales with cell volume, as shown for cells growing on substrates of varying stiffness (gray circles), on a glass substrate with restricted available spread area using micropatterns (blue squares), on a soft substrate with osmotic compression (shear modulus of 100 Pa, green upside down triangles), on an unpatterned (red triangles) and a micropatterned glass substrate (yellow diamonds) with osmotic compression, and on a glass substrate with 10 μM blebbistatin treatment (cyan pentagon) or depleted of ATP (black triangle). Solid line shows the power-law fitting of the data, scales as V^{-2}. Dashed line shows fitting to $G \propto k_B TVI(V - V_{min})^2$ Error bars represent the SD ($n > 200$ individual cells). osm. comp., osmotic compression; pat., patterned.

change. The data shown here are all obtained for a single cell type, A7; however, similar scaling behavior between cell stiffness and cell volume is observed for each cell type, although they are shifted in amplitude and volume (Fig. S4).

Interestingly, if we restrict the data to those cell volumes physiologically accessible without application of external osmotic pressure, where cells solely respond to either changes in substrate stiffness or spread area, the behavior is consistent with $G \propto 1/V^2$, as shown by the solid line in Fig. 5*E*. Intriguingly, this is very similar to the behavior of biopolymer networks reconstituted from either actin or vimentin, where the shear modulus is approximately proportional to the square of the concentration (31–34). This would be expected if the change in the shear modulus is due solely to the water exchange responsible for the volume change. If the data for all measured volumes are included, the full behavior is well described by $G \propto k_BTV/(V - V_{min})^2$, as shown by the dashed line in Fig. 5*E*. While there is no model that predicts this behavior for the shear modulus, it is nevertheless identical in functional form to the behavior of the bulk modulus over the same range of volumes, $B \propto k_BTV/(V - V_{min})^2$. This functional form for the bulk modulus is a direct consequence of the measured *P*–*V* relationship of the cell, which reflects the effects of increased molecular crowding as water is drawn from the cell. Thus, our results suggest that a similar crowding phenomenon is also responsible for the change in the cortical shear modulus under various perturbations that we tested here. Similarly, both osmotic bulk modulus and cytoplasmic shear modulus across multiple perturbations are also observed to be universally dependent on cell volume (Fig. S5), as they do under osmotic compression shown in Fig. 1*A*.

To explore the generality of the correlation between cell stiffness and cell volume, we also include the data with actomyosin contraction inhibited through addition of blebbistatin; we find that cortical stiffness and volume remain exactly on the same functional curve, as shown by the cyan pentagon in Fig. 5*E*. Similarly, when ATP is completely depleted, the data exhibit the same behavior, as shown by the black triangle in Fig. 5*E*. Interestingly, not only for isolated cells, similar behavior is also observed for cells in a 2D monolayer. We grow epithelia MCF10-A cells into a monolayer, but with different cell densities, and measure the corresponding cell volume and cortical shear modulus; we find that cell volume decreases as the density of cells increases (Fig. S4*B*). Cell volume and stiffness again remain correlated: As cell density increases, cell volume decreases, and cortical stiffness increases in a fashion consistent with a $1/V^2$ dependence. These results imply that cell volume plays role in determining cell mechanics, even for cells in confluent layers.

Nuclear Volume Tracks Cell Volume. The nuclear envelope, like the cell membrane, is selectively permeable and allows water exchange; therefore, we wonder if water efflux from the cell extends to the nucleus. To test this, we fluorescently label cell nuclei and use 3D confocal microscopy to measure their volume. We find that cell nuclear volume tracks cell volume both for cells grown under isotonic conditions on different substrates and also for cells whose volume is changed through external osmotic pressure (12), as shown in Fig. 6. This suggests that the cell nucleus also becomes more crowded as cell volume decreases, and this has a direct consequence on the degree of motion within the nucleus. To illustrate this, we measure fluctuating motion of GFP-tagged histone H2B, which is widely used to report on positional fluctuations of chromatin (35, 36); we calculate their mean-squared displacement and find a marked reduction in the level of fluctuations as molecular crowding is increased through an external osmotic pressure (9, 20, 37) (Fig. 6*B*).

Stem-Cell Fate Can Be Directed by Changing Cell Volume. Of the many properties of cells that vary with cell stiffness (38), cell spread area (39), and substrate stiffness (40), one of the most consequential is stem-cell differentiation. We therefore investigate the impact of cell volume on stem-cell differentiation, since cell volume is intrinsically related to cell stiffness, as well as the other parameters like molecular crowding. To do so, we externally impose changes in cell volume through osmotic compression; this results in changes of cell stiffness, but not spread area or substrate properties. Moreover, we confirm that this does not change the tension within the cell, as measured by the traction force microscopy (TFM) (ref. 41; Fig. S6). We grow mMSCs on two different PA gel substrates, one a stiff substrate with a shear modulus of 7 kPa and the other a soft substrate with a shear modulus of 0.2 kPa. On a soft substrate, cells typically have a larger volume than cells on a stiff substrate; thus, we apply additional osmotic pressure by adding 0.1 M PEG 300 (+100 mOsm) to the medium so that the volume of cells grown on the soft gel matches that of the cells grown on the stiff gel (Fig. 7 *D* and *E*). We find that when volumes are matched, cell stiffnesses are also matched (Fig. 7*F*). We expose the cells to bipotential differentiation medium that is supportive of both osteogenic and adipogenic fates (*SI Materials and Methods*). After 1 wk of culture, we observe substantially increased osteogenic differentiation, as indicated by alkaline phosphatase (ALP) activity on the rigid substrate, compared with unperturbed cells on soft substrate, as expected (40). Unexpectedly, osmotically compressed cells grown on the soft substrate also exhibit enhanced ALP activity, suggesting preferential osteogenic differentiation (Fig. 7 *A* and *B*). This is confirmed by Western analysis of the expression of osteogenic biomarkers runt-related transcription factor 2 (RUNX2) and bone sialoprotein (BSP), as shown in Fig. 7*C*.

As a contrapositive test, we use hypotonic conditions (−80 mOsm) to swell cells grown on a stiff substrate, such that both cell volume and nuclear volume match those of cells grown on a soft substrate (Fig. 7 *J* and *K*). We again find that when volumes are matched, cell stiffnesses are matched (Fig. 7*L*). In this case, we observe substantial adipogenic differentiation as shown by in situ staining of neutral lipid accumulation [Oil Red O (ORO)] and the expression of adipogenic biomarker peroxisome proliferator-activated receptor gamma (PPAR-γ) (Fig. 7 *G*–*I*). The results indicate that we can influence stem-cell differentiation either toward osteogenic or adipogenic fates by changing their volume; this suggests that the intranuclear and possibly intracellular crowding affects stem-cell fate.

Stem-Cell Fate Affects Cell Volume. In the absence of strong chemical cues, physical properties such as substrate stiffness or external osmotic pressure affect stem-cell differentiation. However, chemical signals can often override these physical cues. While we have shown that physical signals change cell volume, we wonder if chemical cues also change cell volume during differentiation. Thus, we grow mMSCs on a soft PA gel, which would bias the cells toward adipogenic differentiation; however, we add supplements (β-glycerol phosphate, ascorbic acid, and dexamethasone) to the medium (details in *Materials and Methods*) to direct the cells toward osteogenic differentiation. The mMSCs undergo osteogenic differentiation under these conditions. Interestingly, we find that cell volume decreases during this process and, surprisingly, even precedes osteogenic differentiation, as shown in Fig. 7*M*. Conversely, we find that cell volume increases when we chemically induce adipogenesis using dexamethasone alone for mMSCs cultured on stiff substrates, as shown in Fig. 7*N*. These results suggest that cell volume and stem-cell differentiation are strongly correlated.

Discussion

The data presented here establish the critical importance of cell volume and molecular crowding in determining cell properties, including cell stiffness and intracellular dynamics. Unlike a

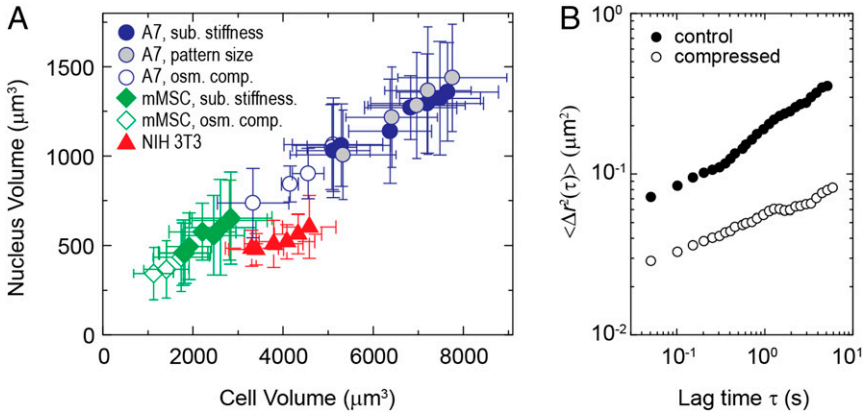

Fig. 6. Cell nuclear volume and nuclear dynamics change with cell volume. (*A*) Nucleus volume always directly tracks cell volume, decreasing proportionally with increasing substrate stiffness, spread area, and osmotic pressure; the ratio between nuclear volume and cell volume remains approximately constant for each tested cell type. (*B*) Mean square displacement of GFP-tagged Histone in MCF-10A cell nuclei, reflecting positional fluctuation of chromatin, significantly reduces under external osmotic compression through application of 0.1 M PEG 300. osm. comp., osmotic compression; sub., substrate.

growing and dividing cell, where volume change is associated with an increase of intracellular protein and other materials, we show that changes in cell volume can alternately be directly associated with changes in intracellular water content while levels of proteins and other materials remain constant: Upon increase of substrate stiffness or cell spread area, cells respond by decreasing their water content and hence increasing their stiffness. While actomyosin contractility is essential for this adaptation, cell contraction itself cannot mechanically change cell volume: The stress generated by the cytoskeleton is too weak (42) (~1–10 kPa, as shown in Fig. S6) to withstand or induce any osmotic pressure difference since pressures are on the order of megapascals (8); therefore, cytoskeletal forces cannot squeeze water out of cells. Instead, it is most likely that contractile tension of the cytoskeleton increases activity of ion channels, which, in turn, affects intercellular water content and hence cell volume (28, 29); this is consistent with our finding that cell volume change is suppressed as we inhibit the activity of specific ion channels and ATP-dependent processes. Surprisingly, both the cortical shear modulus and the cell bulk modulus exhibit exactly the same functional form with cell volume, as shown by Fig. S5. The origin of this behavior for the bulk modulus can be understood as a consequence of molecular crowding; however, the underlying origin of the behavior for the cortical shear modulus is unclear, although the behavior in the physiologically accessible volumes is consistent with the concentration dependence of reconstituted networks, and hence with water content.

Our results also indicate that changing protein concentration has major implications for cell physiology, typified by the effect cell volume change has on stem-cell differentiation. Changes in intracellular water content will change intracellular molecular crowding and cellular dynamics (Fig. 6 and Fig. S7). This will undoubtedly cause significant variations in many internal physiological processes, such as protein folding and binding kinetics (7, 43–45), structural rearrangements and transport phenomena (8, 9, 44), and protein expression patterns (2, 6, 46). Moreover, similar effects extend into the nucleus since the volume of the cell nucleus decreases as cell volume decreases (Fig. 6*A*). This will change the intranuclear molecular crowding, and possibly lamin concentration, which has been suggested to affect chromatin structure, mobility, and therefore transcription and gene expression patterns (10, 47). Thus, cell volume and cell nuclear volume, which are defined features of the cell, may change in physiological conditions such as under tissue compression and osmotic variance in the body, therefore significantly impacting myriad cellular processes, such as signaling, protein dynamics, and even stem-cell differentiation.

Materials and Methods

Cell Culture and Pharmacological Interventions. Cell culture protocol and pharmacological interventions are described in *SI Materials and Methods*. Cells are synchronized to avoid cell size growth and volume change during cell cycle.

Cell Labeling and Immunofluorescence. Cells for confocal imaging are plated at a density of 20 cells per mm^2. Live cells are fluorescently labeled with CellTracker, CellMask plasma membrane stains (Invitrogen), and DRAQ5 (Cell Signaling Technology) to label cytoplasm, membrane, and cell nucleus, respectively. The cells are imaged and sectioned at 0.15-μm intervals by using excitation from a 633- or 543-nm laser or a 488-nm line of an argon laser and a 63×, 1.2-NA water immersion objective on a laser scanning confocal microscope (TCS SP5; Leica). To label actin cortex and get a better resolution of cell boundary and cell size, living cells cultured on substrates are fixed, and their actin structures are labeled by using phalloidin.

Fabrication of PA Gel Substrate and Micropatterned Islands. The fabrication of PA gel substrates with different stiffness and micropatterned islands follows standard procedures (24) and is described in *SI Materials and Methods*.

The 3D Volume Measurement. Stained cells are observed by using a 63×/1.2-NA water immersion lens on a Leica TSC SP5. Cells that we observe are randomly selected. Optical cross-sections are recorded at 0.15-μm *z*-axis intervals to show intracellular, nuclear, and cortical fluorescence. By using theoretical point spread function, a stack of gray-level images (8 bits) are subjected to deconvolution before 3D visualization. The 3D visualization is carried out by using ImageJ and AMIRA software. The volume is calculated by counting voxel number, after thresholding the stack. The confocal measurement has been previously compared with AFM; results from two techniques agree. More details are in *SI Materials and Methods*.

Super-resolution SIM imaging of fixed cells is performed on a microscope (ELYRA SIM; Carl Zeiss) with an Apochromat 63×/1.4-NA oil objective lens (Fig. S1). We use a voxel size of 40 × 40 × 110 nm; the cell height and cell volume measurements from confocal and SIM do not show statistical difference, as shown in Fig. S1.

Osmotic Compression. Hyperosmotic stress is applied by adding PEG 300 to isotonic culture medium. Cells are then allowed to equilibrate in PEG solution for 10 min at 37 °C and 5% CO_2, before measurements. The cell size decreases within 20 s and maintains the small volume for hours, as shown in Movie S1.

Cortical Stiffness Measurements. The mechanical properties of the cell cortex are probed by using OMTC, which is a high-throughput tool for measuring adherent cell mechanics with high temporal and spatial resolution (16, 48, 49). Measurements are done at 37 °C. Measurements of cortical stiffness using OMTC agree with values obtained by other methods such as AFM (50). Frequency-dependent shear moduli of A7 cells in isotonic medium are shown in Fig. S3. For convenience, in this work, we use cortex shear modulus measured at

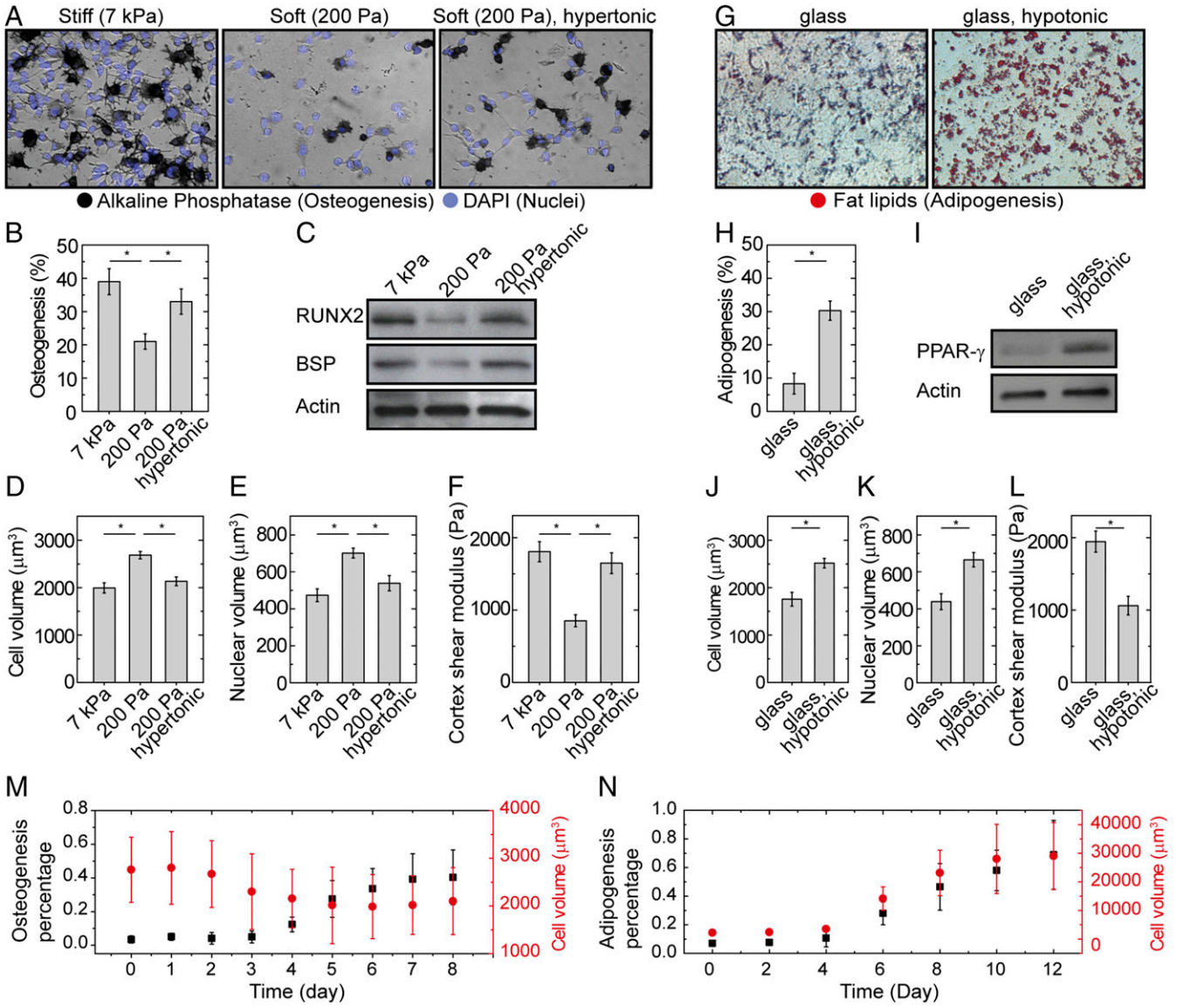

Fig. 7. Cell volume affects differentiation of mMSCs. (*A–F*) Osteogenesis. (*A*) In situ staining of mMSC for ALP (black) and nucleus (DAPI, blue) after 1 wk of culture in the presence of combined osteogenic and adipogenic chemical supplements shows increased osteogenesis on the stiff substrate (shear modulus of 7 kPa) and the soft substrate (shear modulus of 200 Pa) with osmotic compression (with 0.1 M PEG 300, additionally to the medium), compared with the control on soft substrate without additional osmotic pressure. (*B*) Mean percentages of mMSC osteogenesis. Error bars, SEM ($n = 3$ samples). *$P < 0.05$. (*C*) Western analysis of osteogenic protein expression (RUNX2 and BSP) in mMSCs after 3 d of culture. (*C–F*) Cell volume (*D*), nucleus volume (*E*), and cortex shear modulus (*F*) measured with confocal microscopy and OMTC, for three experimental conditions ($n > 50$ individual cells). *$P < 0.05$. (*G–L*) Adipogenesis. (*G*) In situ staining of mMSC for fat lipids (red) after 2 wk of culture in the presence of combined osteogenic and adipogenic chemical supplements shows enhanced adipogenesis on stiff substrate with application of hypotonic pressure (with the addition of 30% DI water), compared with the control. (*H*) Mean percentages of mMSC adipogenesis. Error bars, SEM ($n = 3$ samples). *$P < 0.05$. (*I*) Western analysis of adipogenesis protein expression (PPAR-γ) in mMSCs after 1 wk of culture. (*J–L*) Cell volume (*J*), nucleus volume (*K*), and cortex shear modulus (*L*) measured with confocal microscopy and OMTC, for three experimental conditions ($n > 50$ individual cells). *$P < 0.05$. (*M*) mMSCs are exposed to osteogenesis medium for 10 d. The ratio of cells expressing high level of ALP, as measured by using Fast Blue staining, as described in *SI Materials and Methods*, is counted in three independent samples fixed each day. Volume of cells is observed each day as well. As the ratio of differentiated cells increases, cell volume decreases correspondingly ($n = 3$ samples; error bars represent SD). (*N*) mMSCs are exposed to adipogenesis medium for 2 wk. The ratio of cells with clear fat lipid accumulation, as visualized by ORO staining, as described in *SI Materials and Methods*, is counted in three independent samples fixed every 2 d. Volume of cells is measured at the same time as well. As the ratio of differentiated cells increases, cell volume increases correspondingly ($n = 3$ samples; error bars represent SD). (Magnification: *A* and *G*, 400×.)

a fixed frequency, 0.75 Hz, for comparison under different microenvironmental conditions. More details are in *SI Materials and Methods*.

Cytoplasmic Material Properties Measured Using Optical Tweezers. To directly measure the micromechanical properties of the cytoplasm, we perform active microrheology measurements using optical tweezers to impose a sinusoidal oscillation on a 500-nm-diameter probe particle microinjected in a cell, as described (17, 20). The trap stiffness we use is calibrated as 0.05 pN/nm. Trapped beads are oscillated across a frequency range of 0.3–70 Hz; the frequency-dependent shear modulus of the cytoplasm is shown in Fig. S3. The data plotted in the lower part of Fig. 1*A* and Fig. S5 are G' measured at 10 Hz under different conditions. More details are in *SI Materials and Methods*.

Stem Cell Culture and Differentiation. The clonally derived murine bone marrow mesenchymal stem cell line originally from BALB/c mice (D1s) are purchased from American Type Cell Culture and are maintained in standard

DMEM and supplemented with 10% FBS and 1% penicillin/streptomycin. They are cultured at no more than 80% confluency at no greater than passage 25 in serum-supplemented DMEM. For experiments, cells are trypsinized and plated on collagen I-coated soft and stiff substrates at a density of 20 cells per mm^2. We then let cells fully attach and spread for 1 h, before applying osmotic pressure and adding bipotential differentiation medium. In the compression sample, we add 0.1 M PEG 300 (100 mOsm) to the medium, so that the volume and stiffness of cells on the soft gel match those of the cells grown on the stiff gel, as measured with confocal and OMTC. Similarly, in the swelling sample on glass, after plating cells, we apply hypotonic pressure by adding 30% deionized water into culture medium. To induce differentiation (51), mMSC cultures are supplemented with 10 mM β-glycerol phosphate (Sigma), 50 μg/mL ascorbic acid (Sigma), and 0.1 μM dexamethasone (Sigma), as dexamethasone alone has demonstrated the ability to induce adipogenesis of D1 in vitro (52). Culture medium with additional osmotic pressures and supplements are exchanged every 3 d.

Western Analysis of MSC Lineage Specification. For Western blots, after 3 d (osteogenesis, as shown in Fig. 7 *A–F*) or 1 wk (adipogenesis, as shown in Fig. 7 *G–L*) of culture, cells are lysed in RIPA buffer (Sigma-Aldrich) with Complete Mini protease inhibitor (Roche). Lysates are centrifuged at 16,000 × *g* at 4 °C for 20 min, and total protein is estimated with a Bradford assay (BCA; Thermo Scientific Inc.). Protein lysates are separated in precast Tris–glycine or –acetate gels and transferred onto nitrocellulose membranes (both Invitrogen). Blots are incubated with primary antibodies at 4 °C overnight. Following washes, blots are incubated with appropriate species-specific secondary antibodies (Jackson ImmunoResearch Laboratories) and chemiluminescence (Thermo Scientific Inc.) is detected by films (Kodak MR; Sigma-Aldrich). Images of Western blots are quantified by using ImageJ software. Actin bands are scanned to normalize for loading differences between samples. Antibodies we use for immunoblotting are mouse anti-RUNX2 antibody, mouse anti-BSP antibody, and mouse anti–PPAR-γ antibody (Abcam), mouse anti-actin antibody (Chemicon), and goat anti-mouse secondary antibody (Jackson Immunoresearch Laboratories).

Immunostaining. After 1 wk (osteogenesis, as shown in Fig. 7 *A–F*) or 2 wk (adipogenesis, as shown in Fig. 7 *G–L*) of culture, cells are fixed with 4% paraformaldehyde and 0.1% Triton X-100 in PBS. For osteogenesis examination, ALP activity is visualized by Fast Blue staining [200 μg/mL naphtol-AS-MX-phosphate (NAMP) combined with 200 μg /mL Fast Blue salt] in alkaline buffer (100 mM Tris·HCl, 100 mM NaCl, 0.1% Tween-20, and 50 mM $MgCl_2$, pH 8.2), as shown in Fig. 7*A*. For adipogenesis examination, fat lipid accumulation is visualized by ORO (600 μg/mL in isopropyl alcohol for 2 h at 25 °C) staining, as shown in Fig. 7*G*. Nuclei are visualized with 2.7 mM DAPI in PBS. The density of ALP-expressing cells and ORO-positive cells are calculated by counting the number of cells in more than three randomly selected fields (10× magnification), and normalizing to the total number of cells detected by DAPI staining, in each individual sample.

TFM. Cell contractility is measured using the TFM technique according to described methods (41, 53, 54). More details are in *SI Materials and Methods*.

ACKNOWLEDGMENTS. We thank J. P. Butler, F. Deng, and A. E. Ehrlicher for helpful discussions. This work was supported by NIH Grants P01GM096971, P01HL120839, and R01EB014703; Harvard Materials Research Science and Engineering Center Grant DMR-1420570; and NSF Grant DMR-1310266. M.H.J. and J.R.M. were supported by NIH Grant HL86655.

1. Hoffmann EK, Lambert IH, Pedersen SF (2009) Physiology of cell volume regulation in vertebrates. *Physiol Rev* 89:193–277.
2. Lang F, et al. (1998) Functional significance of cell volume regulatory mechanisms. *Physiol Rev* 78:247–306.
3. Tzur A, Kafri R, LeBleu VS, Lahav G, Kirschner MW (2009) Cell growth and size homeostasis in proliferating animal cells. *Science* 325:167–171.
4. Habela CW, Ernest NJ, Swindall AF, Sontheimer H (2009) Chloride accumulation drives volume dynamics underlying cell proliferation and migration. *J Neurophysiol* 101: 750–757.
5. Watkins S, Sontheimer H (2011) Hydrodynamic cellular volume changes enable glioma cell invasion. *J Neurosci* 31:17250–17259.
6. Ellis RJ (2001) Macromolecular crowding: Obvious but underappreciated. *Trends Biochem Sci* 26:597–604.
7. Minton AP (2001) The influence of macromolecular crowding and macromolecular confinement on biochemical reactions in physiological media. *J Biol Chem* 276: 10577–10580.
8. Zhou EH, et al. (2009) Universal behavior of the osmotically compressed cell and its analogy to the colloidal glass transition. *Proc Natl Acad Sci USA* 106:10632–10637.
9. Oh D, Zidovska A, Xu Y, Needleman DJ (2011) Development of time-integrated multipoint moment analysis for spatially resolved fluctuation spectroscopy with high time resolution. *Biophys J* 101:1546–1554.
10. Irianto J, et al. (2013) Osmotic challenge drives rapid and reversible chromatin condensation in chondrocytes. *Biophys J* 104:759–769.
11. Moeendarbary E, et al. (2013) The cytoplasm of living cells behaves as a poroelastic material. *Nat Mater* 12:253–261.
12. Swanson JA, Lee M, Knapp PE (1991) Cellular dimensions affecting the nucleocytoplasmic volume ratio. *J Cell Biol* 115:941–948.
13. Xiong F, et al. (2014) Interplay of cell shape and division orientation promotes robust morphogenesis of developing epithelia. *Cell* 159:415–427.
14. Fischer-Friedrich E, Hyman AA, Jülicher F, Müller DJ, Helenius J (2014) Quantification of surface tension and internal pressure generated by single mitotic cells. *Sci Rep* 4: 6213.
15. Alberts B, Wilson JH, Hunt T (2008) *Molecular Biology of the Cell* (Garland Science, New York).
16. Fabry B, et al. (2001) Scaling the microrheology of living cells. *Phys Rev Lett* 87:148102.
17. Guo M, et al. (2013) The role of vimentin intermediate filaments in cortical and cytoplasmic mechanics. *Biophys J* 105:1562–1568.
18. Trepat X, et al. (2005) Thrombin and histamine induce stiffening of alveolar epithelial cells. *J Appl Physiol (1985)* 98:1567–1574.
19. Overby DR, et al. (2014) Altered mechanobiology of Schlemm's canal endothelial cells in glaucoma. *Proc Natl Acad Sci USA* 111:13876–13881.
20. Guo M, et al. (2014) Probing the stochastic, motor-driven properties of the cytoplasm using force spectrum microscopy. *Cell* 158:822–832.
21. Discher DE, Janmey P, Wang YL (2005) Tissue cells feel and respond to the stiffness of their substrate. *Science* 310:1139–1143.
22. Dupont S, et al. (2011) Role of YAP/TAZ in mechanotransduction. *Nature* 474:179–183.
23. Solon J, Levental I, Sengupta K, Georges PC, Janmey PA (2007) Fibroblast adaptation and stiffness matching to soft elastic substrates. *Biophys J* 93:4453–4461.
24. Pelham RJ, Jr, Wang Yl (1997) Cell locomotion and focal adhesions are regulated by substrate flexibility. *Proc Natl Acad Sci USA* 94:13661–13665.
25. Chen CS, Mrksich M, Huang S, Whitesides GM, Ingber DE (1997) Geometric control of cell life and death. *Science* 276:1425–1428.
26. Stewart MP, et al. (2011) Hydrostatic pressure and the actomyosin cortex drive mitotic cell rounding. *Nature* 469:226–230.
27. Cooper KL, et al. (2013) Multiple phases of chondrocyte enlargement underlie differences in skeletal proportions. *Nature* 495:375–378.
28. Matthews BD, Thodeti CK, Ingber DE (2007) Activation of mechanosensitive ion channels by forces transmitted through integrins and the cytoskeleton. *Mechanosensitive Ion Channels, Part A*, Current Topics in Membranes, ed Hamill OP (Elsevier Academic, San Diego), Vol 58, pp 59–85.
29. Wiggins P, Phillips R (2005) Membrane-protein interactions in mechanosensitive channels. *Biophys J* 88:880–902.
30. Zhang W, et al. (2015) Ankyrin repeats convey force to gate the NOMPC mechanotransduction channel. *Cell* 162:1391–1403.
31. Lin Y-C, et al. (2010) Origins of elasticity in intermediate filament networks. *Phys Rev Lett* 104:058101.
32. Gardel ML, et al. (2004) Elastic behavior of cross-linked and bundled actin networks. *Science* 304:1301–1305.
33. MacKintosh FC, Käs J, Janmey PA (1995) Elasticity of semiflexible biopolymer networks. *Phys Rev Lett* 75:4425–4428.
34. Satcher RL, Jr, Dewey CF, Jr (1996) Theoretical estimates of mechanical properties of the endothelial cell cytoskeleton. *Biophys J* 71:109–118.
35. Zidovska A, Weitz DA, Mitchison TJ (2013) Micron-scale coherence in interphase chromatin dynamics. *Proc Natl Acad Sci USA* 110:15555–15560.
36. Kimura H, Cook PR (2001) Kinetics of core histones in living human cells: Little exchange of H3 and H4 and some rapid exchange of H2B. *J Cell Biol* 153:1341–1353.
37. Miermont A, et al. (2013) Severe osmotic compression triggers a slowdown of intracellular signaling, which can be explained by molecular crowding. *Proc Natl Acad Sci USA* 110:5725–5730.
38. Chowdhury F, et al. (2010) Material properties of the cell dictate stress-induced spreading and differentiation in embryonic stem cells. *Nat Mater* 9:82–88.
39. McBeath R, Pirone DM, Nelson CM, Bhadriraju K, Chen CS (2004) Cell shape, cytoskeletal tension, and RhoA regulate stem cell lineage commitment. *Dev Cell* 6:483–495.
40. Engler AJ, Sen S, Sweeney HL, Discher DE (2006) Matrix elasticity directs stem cell lineage specification. *Cell* 126:677–689.
41. Butler JP, Tolić-Nørrelykke IM, Fabry B, Fredberg JJ (2002) Traction fields, moments, and strain energy that cells exert on their surroundings. *Am J Physiol Cell Physiol* 282: C595–C605.
42. Wang N, Ostuni E, Whitesides GM, Ingber DE (2002) Micropatterning tractional forces in living cells. *Cell Motil Cytoskeleton* 52:97–106.
43. Ball P (2008) Water as an active constituent in cell biology. *Chem Rev* 108:74–108.
44. Boersma AJ, Zuhorn IS, Poolman B (2015) A sensor for quantification of macromolecular crowding in living cells. *Nat Methods* 12:227–229.
45. Dhar A, et al. (2010) Structure, function, and folding of phosphoglycerate kinase are strongly perturbed by macromolecular crowding. *Proc Natl Acad Sci USA* 107: 17586–17591.
46. Robbins E, Pederson T, Klein P (1970) Comparison of mitotic phenomena and effects induced by hypertonic solutions in HeLa cells. *J Cell Biol* 44:400–416.
47. Swift J, et al. (2013) Nuclear lamin-A scales with tissue stiffness and enhances matrix-directed differentiation. *Science* 341:1240104.

48. Mijailovich SM, Kojic M, Zivkovic M, Fabry B, Fredberg JJ (2002) A finite element model of cell deformation during magnetic bead twisting. *J Appl Physiol (1985)* 93: 1429–1436.
49. Fabry B, et al. (2001) Selected contribution: Time course and heterogeneity of contractile responses in cultured human airway smooth muscle cells. *J Appl Physiol (1985)* 91:986–994.
50. Byfield FJ, et al. (2009) Absence of filamin A prevents cells from responding to stiffness gradients on gels coated with collagen but not fibronectin. *Biophys J* 96: 5095–5102.
51. Huebsch N, et al. (2010) Harnessing traction-mediated manipulation of the cell/matrix interface to control stem-cell fate. *Nat Mater* 9:518–526.
52. Li X, Jin L, Cui Q, Wang GJ, Balian G (2005) Steroid effects on osteogenesis through mesenchymal cell gene expression. *Osteoporos Int* 16:101–108.
53. Pelham RJ, Jr, Wang Yl (1999) High resolution detection of mechanical forces exerted by locomoting fibroblasts on the substrate. *Mol Biol Cell* 10:935–945.
54. Tolić-Nørrelykke IM, Butler JP, Chen J, Wang N (2002) Spatial and temporal traction response in human airway smooth muscle cells. *Am J Physiol Cell Physiol* 283: C1254–C1266.
55. Kasza KE, et al. (2009) Filamin A is essential for active cell stiffening but not passive stiffening under external force. *Biophys J* 96:4326–4335.
56. Engler A, et al. (2004) Substrate compliance versus ligand density in cell on gel responses. *Biophys J* 86:617–628.
57. Cunningham CC, et al. (1992) Actin-binding protein requirement for cortical stability and efficient locomotion. *Science* 255:325–327.
58. Straight AF, et al. (2003) Dissecting temporal and spatial control of cytokinesis with a myosin II Inhibitor. *Science* 299:1743–1747.
59. Thery M, Piel M (2009) Adhesive micropatterns for cells: A microcontact printing protocol. *Cold Spring Harb protoc* 2009:pdb.prot5255.
60. Xia YN, Whitesides GM (1998) Soft lithography. *Angew Chem Int Ed* 37:551–575.
61. Moller W, Roth C, Stahlhofen W (1990) Improved spinning top aerosol generator for the production of high concentrated ferrimagnetic aerosols. *J Aerosol Sci* 21(Suppl 1): S657–S660.
62. Veigel C, Bartoo ML, White DCS, Sparrow JC, Molloy JE (1998) The stiffness of rabbit skeletal actomyosin cross-bridges determined with an optical tweezers transducer. *Biophys J* 75:1424–1438.